Cell Metabolism
Article

Glucose-Independent Glutamine Metabolism via TCA Cycling for Proliferation and Survival in B Cells

Anne Le,[1,*] Andrew N. Lane,[6,8,*] Max Hamaker,[2] Sminu Bose,[1] Arvin Gouw,[3] Joseph Barbi,[4] Takashi Tsukamoto,[5] Camilio J. Rojas,[5] Barbara S. Slusher,[5] Haixia Zhang,[9] Lisa J. Zimmerman,[9] Daniel C. Liebler,[9] Robbert J.C. Slebos,[9] Pawel K. Lorkiewicz,[6] Richard M. Higashi,[6,7] Teresa W.M. Fan,[6,7,8,*] and Chi V. Dang[10,*]
[1]Division of Gastrointestinal and Liver Pathology, Department of Pathology
[2]Division of Hematopathology, Department of Pathology
[3]Graduate Program in Pathobiology, Department of Pathology
[4]Division of Immunology and Hematopoiesis, Department of Oncology
[5]Neurology and Brain Science Institute
Johns Hopkins University School of Medicine, Baltimore, MD 21205, USA
[6]Center for Regulatory and Environmental Analytical Metabolomics
[7]Department of Chemistry
[8]J.G. Brown Cancer Center
University of Louisville, Louisville, KY 40202, USA
[9]Biochemistry Jim Ayers Institute for Precancer Detection and Diagnosis, Vanderbilt University Medical School, Nashville, TN 37232-8575, USA
[10]Abramson Cancer Center of the University of Pennsylvania, Philadelphia, PA 19104, USA
*Correspondence: annele@jhmi.edu (A.L.), anlane01@louisville.edu (A.N.L.), twmfan@gmail.com (T.W.M.F.), dangvchi@exchange.upenn.edu (C.V.D.)
DOI 10.1016/j.cmet.2011.12.009

SUMMARY

Because MYC plays a causal role in many human cancers, including those with hypoxic and nutrient-poor tumor microenvironments, we have determined the metabolic responses of a MYC-inducible human Burkitt lymphoma model P493 cell line to aerobic and hypoxic conditions, and to glucose deprivation, using stable isotope-resolved metabolomics. Using [U-^{13}C]-glucose as the tracer, both glucose consumption and lactate production were increased by MYC expression and hypoxia. Using [U-^{13}C,^{15}N]-glutamine as the tracer, glutamine import and metabolism through the TCA cycle persisted under hypoxia, and glutamine contributed significantly to citrate carbons. Under glucose deprivation, glutamine-derived fumarate, malate, and citrate were significantly increased. Their ^{13}C-labeling patterns demonstrate an alternative energy-generating glutaminolysis pathway involving a glucose-independent TCA cycle. The essential role of glutamine metabolism in cell survival and proliferation under hypoxia and glucose deficiency makes them susceptible to the glutaminase inhibitor BPTES and hence could be targeted for cancer therapy.

INTRODUCTION

Mutations of genes involved in the tricarboxylic acid (TCA) cycle, such as fumarate hydratase, succinate dehydrogenase, or isocitrate dehydrogenase 1 or 2, are causally linked to familial cancer syndromes (Bensaad et al., 2006) or spontaneous low-grade gliomas and acute myelogenous leukemia (Dang et al., 2010). Together with the well-known Warburg effect (Koppenol et al., 2011; Vander Heiden et al., 2009; Warburg, 1956; Warburg et al., 1924) and numerous other alterations in the central metabolism of cancers (King et al., 2006; Samudio et al., 2009), these all point to the important role of metabolism in the development of many cancers and its therapeutic opportunities (Vander Heiden, 2011). Further, tumor suppressors such as p53 and oncogenes such as *MYC* and *RAS* have been directly linked to regulating metabolic pathways (Dang et al., 2009a; Telang et al., 2007) for initiating tumorigenesis and tumor progression. These genetic changes correlate with an increase in glucose consumption and lactate production when MYC is high. However, solid tumors contain regions that are both hypoxic and glucose depleted (Schroeder et al., 2005), requiring alternative strategies for survival and/or proliferation.

Here, we report stable isotope-resolved metabolomic (SIRM) studies of MYC-induced alterations in glucose and glutamine metabolism, in which we find persistent, MYC-dependent hypoxic metabolism of glutamine, even in the absence of glucose. Using NMR and MS, we have traced the fates of individual atoms from uniformly ^{13}C-labeled glucose ([U-^{13}C]-Glc) or ^{13}C,^{15}N-labeled glutamine ([U-^{13}C,^{15}N]-Gln) in human B cell P493 cells carrying an inducible *MYC* vector. Overexpressed MYC resulted in the concurrent conversion of glucose to lactate and the oxidation of glutamine via the TCA cycle. Under hypoxic conditions with high MYC, a substantial fraction of the glucose consumed was converted to excreted lactate, and glutamine continued to be utilized by the TCA cycle, which was used for cell survival. We further document the finding of a fully ^{13}C-labeled citrate isotopologue that contained carbons deriving completely from

labeled glutamine, suggesting the existence of a glucose-independent TCA cycle. We also found under glucose-depleted culture conditions that a glutamine-dependent and glucose-independent TCA cycle may operate under both aerobic and hypoxic conditions. Moreover, we observed an enhanced conversion of glutamine to glutathione under hypoxia; glutathione is an important reducing agent for controlling the accumulation of mitochondrial reduced oxygen species (ROS). Under moderate hypoxia, excess ROS is generated at complex II owing to a mismatch between NADH production and terminal oxidase activity (Wu et al., 2007). We therefore tested whether inhibition of glutamine metabolism could induce oxidative stress under hypoxia. We found that inhibition of glutaminase (GLS) by the glutaminase-selective inhibitor BPTES (Robinson et al., 2007) elevated ROS levels and diminished ATP levels in hypoxic cells. In fact, we found that inhibition of glutaminase effectively kills hypoxic cancer cells in vitro and delays tumor xenograft growth in vivo.

RESULTS

Coexistence of Oxidative and Aerobic Glycolysis

Our genomic analysis of MYC target genes indicates that the expression of genes involved in glycolysis and in mitochondrial respiration is coregulated by MYC (Dang, 2010; Kim et al., 2007, 2008; Li et al., 2005). We thus determined the metabolic consequences of MYC activation in a model cell line (P493) of human Burkitt lymphoma grown in uniformly labeled [U-^{13}C]-Glc under aerobic (21% O_2) or hypoxic (1% O_2) conditions. Although the levels of metabolites at steady state are the result of the balance between production and consumption, the use of SIRM enabled us to determine not only steady levels of metabolites but also the isotopomer and isotopologue distributions of metabolites derived from ^{13}C-labeled glucose for reconstruction of metabolic pathways. Time course isotopomer data on extracellular metabolites further provided flux measurement for substrate import and product release (Figure 1A, see Figures S2C and S3B and Table S1 available online). P493 cells contain a tetracycline-repressible *MYC* construct, such that tetracycline withdrawal results in rapid induction of MYC and tetracycline treatment results in MYC suppression (Figure S1A). Induction of MYC resulted in an increase of ^{13}C-glucose consumption and ^{13}C-lactate production, which were further accentuated by hypoxia (Figure 1A). NMR analysis of ^{13}C-labeled metabolites derived from [U-^{13}C]-Glc in cell extracts also corroborated the finding that overexpressed MYC resulted in lactic fermentation even under aerobic conditions (Figure 1B). The same cell extracts were further analyzed by GC-MS to quantify glucose-derived ^{13}C isotopologues of lactate (lactate with different number of ^{13}C atoms) (Figure 1D). Levels of the m+3 isotopologue of lactate (triply ^{13}C-labeled lactate or $^{13}C_3$-lactate) derived from glucose shown with MYC ON or OFF in aerobic (A) or hypoxic (H) conditions (Figure 1D) also support the ability of MYC to increase aerobic glycolysis (Figure 1C). Under hypoxic conditions, glucose-derived lactate was increased but was less dependent on MYC. The production of lactate (Table S1) accounts for only part of the glucose consumed. Although a complete carbon inventory has not been achieved, we estimate that a significant fraction of the glucose enters new biomass, which with respiration is associated with carbon loss as CO_2.

As shown in Figure 2, glucose-derived TCA cycle intermediates under aerobic condition displayed a dependence on MYC, such that the doubly ^{13}C-labeled isotopologue of citrate ($^{13}C_2$-citrate), succinate, fumarate, and malate (m+2 forms, circled red) increased when MYC was ON. Glucose-derived α-ketoglutarate (m+2), which was at very low cellular concentration, also demonstrated a dependence on MYC; it was only detectable when MYC was ON. Hypoxia decreased the MYC-induced conversion of glucose to citrate (m+2) and to other m+2 isotopologues of TCA cycle intermediates (malate, fumarate, and succinate), but these activities were independent of MYC expression (MYC ON-H versus MYC OFF-H). In addition to the synthesis of $^{13}C_2$-citrate, there was a significant production of $^{13}C_5$-citrate (m+5, circled green) with MYC ON under aerobic conditions. This citrate isotopologue could be produced from m+2 acetyl-CoA plus m+3 oxaloacetate (product of pyruvate carboxylation, green arrow and circles, Figure 2) (Fan et al., 2010), and its level appeared to be attenuated by hypoxia and the absence of ectopic MYC (Tet treatment). It is notable that a large fraction (up to 70%) of these TCA metabolites (m+0) were not derived from the labeled glucose, suggesting an alternative source and/or prolonged half-lives of these metabolites that could have existed prior to the administration of labeled glucose.

Persistence of Glutamine Oxidation via the TCA Cycle under Hypoxia

The attenuation of glucose entry into the TCA cycle under hypoxia (Figure 2) is consistent with the hypoxia inducible factor (HIF)-mediated diversion of pyruvate to lactate (away from acetyl-CoA) through the induction of LDHA (which increases the relative flux from pyruvate to lactate) and PDK1 (which decreases the relative flux from pyruvate to acetyl-CoA) (Kim et al., 2006). Because it was previously documented that MYC induces glutamine metabolism under aerobic conditions (Gao et al., 2009; Wise et al., 2008), we sought to determine whether glutamine entry into the TCA cycle would also be compromised by hypoxia.

Using [U-^{13}C,^{15}N]-Gln ($^{13}C_5{}^{15}N_2$-Gln) as the tracer with SIRM analysis, the fates of glutamine as a function of MYC induction and oxygen availability were determined (Figures 3B–3D). Glutamine is transported into cells by transporters, such as the direct targets of MYC SLC1A5 or ASCT2 (Figure S1C), and then converted to glutamate by glutaminase (GLS, kidney isoform, which is also a target of MYC) (Figure S1D). $^{13}C_5{}^{15}N_2$-Gln (m+7) is converted by glutaminase into $^{13}C_5{}^{15}$N-Glu (m+6) plus $^{15}NH_4{}^+$ (Figure 3A). NMR studies of biological replicate experiments revealed a MYC-dependent conversion of labeled glutamine to glutamate, which unexpectedly persisted in hypoxia (Figure 3B). This result was corroborated by the GC-MS analysis of the same set of polar extracts. Intracellular glutamine was converted to glutamate (m+6 isotopologue or $^{13}C_5{}^{15}N_1$-Glu, Figure 3D) in a MYC-dependent fashion that persisted under hypoxia. A large fraction of the m+5 glutamate isotopologue was also present and displayed a similar MYC and hypoxia dependence as the m+6 isotopologue. The m+5 isotopologue of glutamate was largely $^{13}C_5$-Glu as determined by high-resolution FT-ICR-MS (Figure S1E), which resolved the neutron mass from

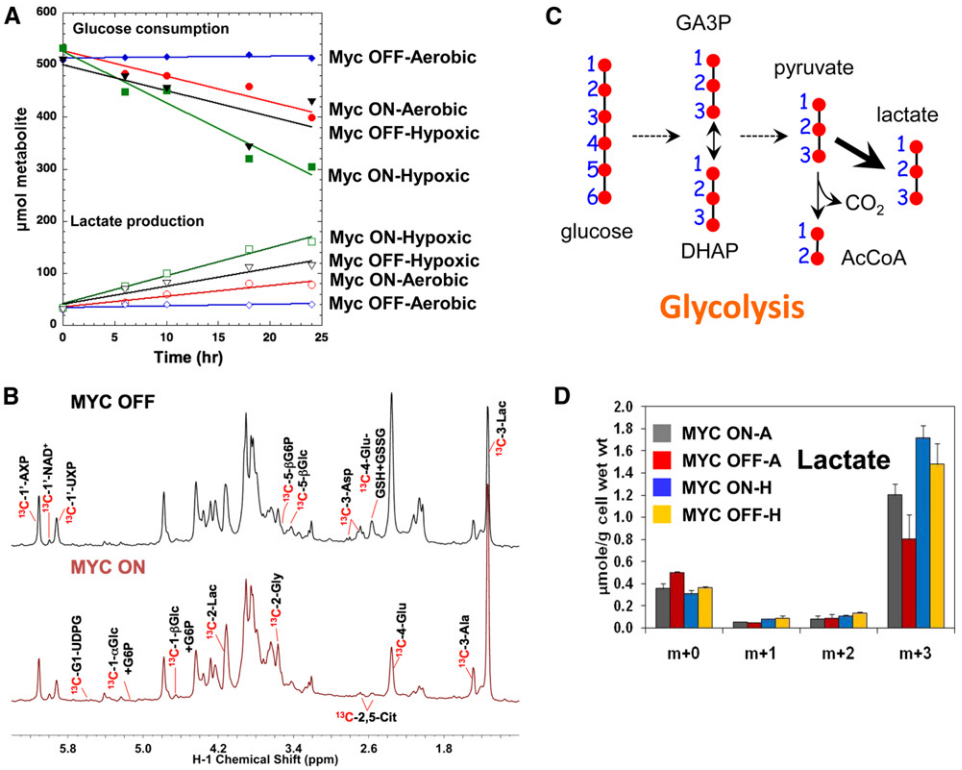

Figure 1. MYC Induces Aerobic Glycolysis that Is Heightened in Hypoxia

(A) Time course of glucose consumption and lactate secretion into the medium. P493 cells were treated with 0.1 μg/ml tetracycline (MYC OFF) or without tetracycline (MYC ON) for 48 hr in hypoxic (H) or aerobic (A) conditions and were grown in RPMI containing 10 mM [U-^{13}C] glucose (^{13}C-Glc$_6$) for 24 hr. Media metabolites and ^{13}C enrichments were measured by 1D ^{1}H NMR. The metabolite amounts are expressed as μmole. Each time data point is an average of duplicate samples. The rates were calculated from linear regression of the time courses and normalized to cell mass as μmole/h/g cells. Open symbols are ^{13}C lactate, filled symbols are ^{13}C glucose. Filled red circles, MYC ON aerobic; blue diamonds, MYC OFF aerobic; green squares, MYC ON hypoxic; black triangles, MYC OFF hypoxic.

(B) 1-D ^{1}H{^{13}C} HSQC NMR spectra of cell extracts of P493 MYC ON versus MYC OFF. Intracellular ^{13}C-lactate synthesized from ^{13}C glucose was attenuated when MYC is off, which was also observed by GC-MS analysis of the same extracts (D). NMR spectra were recorded at 800 MHz and 20°C. Each ^{1}H peak arose from protons directly attached to ^{13}C, and the peak assignment denotes the ^{13}C-carbon. Thus, the peak intensity reflects ^{13}C abundance of the attached carbon.

(C) Diagram of ^{13}C-labeling patterns of glycolytic products with ^{13}C$_6$-Glc as tracer. Glucose with carbons (red circles) labeled at all six positions (blue) generates ^{13}C$_3$-lactate via pyruvate (three carbons), which also produces ^{13}C$_2$-acetyl CoA.

(D) GC-MS analysis of MYC and/or hypoxia effect on ^{13}C-Glc$_6$ metabolism to different ^{13}C isotopologues of lactate. Overexpressed MYC enhanced lactate production (most notably ^{13}C$_3$-lactate; m+3), and hypoxia further increased labeled incorporation into lactate. Each value is an average of duplicate samples. The error bars represent SEM.

^{13}C and ^{15}N. ^{13}C$_5$-Glu should be a transamination product of ^{13}C-labeled glutamine-derived α-ketoglutarate (α-KG) with unlabeled nitrogen sources (Figure 3A). α-ketoglutarate levels also tracked MYC expression (Figure 4). Furthermore, the dependence of glutaminase activity on MYC expression measured in extracts suggests that the intracellular conversion of labeled glutamine to glutamate is at least partly regulated by GLS1 activity in response to MYC (Figure S2A). This was further supported by the higher level of ammonium ions—the other product of the glutaminase reaction—that were released into the medium under MYC ON conditions (Figure S2B).

Levels of fully labeled glutamine in the media were measured to determine the rate of consumption of glutamine. Glutamine consumption rates were in the following order: MYC ON aerobic ≈MYC ON hypoxic > MYC OFF hypoxic > MYC OFF aerobic (Figure 3C, Figure S2C). The m+5 and m+6 isotopologues of glutamate were also present in the medium (Figure 3C), which reflects exchange of intracellular glutamine-derived glutamate for other amino acids such as cystine (see below).

As depicted in Figure 3A, labeled glutamine catabolism by glutaminase led to the production of ^{13}C$_5$-αKG, which can enter the TCA cycle for further oxidation. As shown in Figure 4, the synthesis of ^{13}C$_4$-succinate, -fumarate, and -malate (m+4) is consistent with the oxidation of ^{13}C$_5$-αKG via the forward reactions of the TCA cycle (red circles, Figure S2D). These labeled TCA intermediates all responded to MYC status by increasing 60% to >100% when MYC was ON, regardless of O_2 availability (Figure 4). The levels of ^{13}C$_4$-citrate, which is synthesized in the second turn from ^{13}C$_4$-oxaloacetate (OAA, derived from labeled glutamine in the first turn) and acetyl-CoA (from unlabeled glucose or other unlabeled sources) by citrate synthase (CS), also responded to MYC expression under both aerobic and hypoxic conditions (Figure 4). These results show that MYC can drive glutamine metabolism around the TCA cycle even under hypoxia.

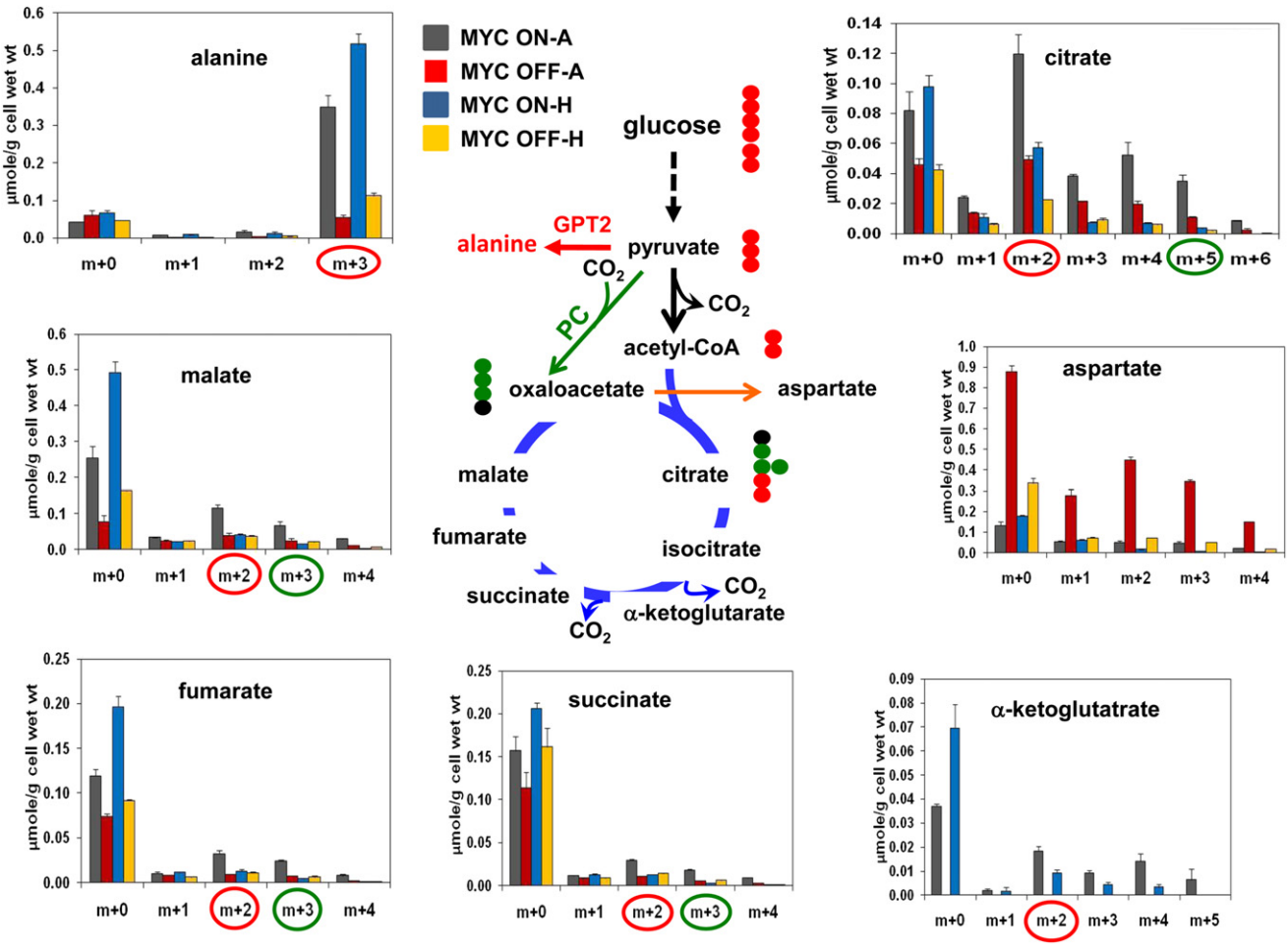

Figure 2. Glucose Entry into the TCA Cycle Is Induced by MYC and Suppressed by Hypoxia

The cycle reactions are depicted without or with pyruvate carboxylation (green arrow), and the ^{13}C isotopomer patterns are the result of one cycle turn. The isotopologue distributions were determined by GC-MS. The incorporation of ^{13}C atoms from $^{13}C_6$-Glc into citrate, α-ketoglutarate (α-KG), succinate, fumarate, and malate are denoted as m+n, where n is the number of ^{13}C atoms. The m+5 ($^{13}C_5$)-citrate (green circle) is produced by condensation of m+2 acetyl-CoA with m+3 OAA (from pyruvate carboxylation), while m+2 ($^{13}C_2$)-citrate is synthesized without input of pyruvate carboxylation. Red and green circles, ^{13}C atoms derived from $^{13}C_6$-Glc without or with pyruvate carboxylation, respectively. GPT2, glutamate-pyruvate transaminase; PC, pyruvate carboxylase; CO_2 indicates where carbon dioxide is released. A, aerobic; H, hypoxic. The error bars represent SEM.

Glucose-Independent Oxidation of Glutamine for Survival and Proliferation

In addition to the production of the $^{13}C_4$-citrate isotopologue, there was a significant formation of other citrate isotopologues, e.g., $^{13}C_3$- (m+3), $^{13}C_5$- (m+5), and $^{13}C_6$-citrate (m+6) (Figure 4). These labeled species indicate that the production of labeled acetyl-CoA and OAA isotopologues from the glutamine tracer are using pathways external to the TCA cycle. Figure S2D depicts the pathways that can lead to the synthesis of $^{13}C_3$-, $^{13}C_5$-, and $^{13}C_6$-citrate. These include the cytoplasmic ATP-citrate lyase (ACL) plus malic enzyme (ME) reactions, which produce, respectively, $^{13}C_4/^{13}C_2$-OAA and $^{13}C_3/^{13}C_2$-pyruvate; the latter yields $^{13}C_2/^{13}C_1$-acetyl-CoA via pyruvate dehydrogenase (PDH). Condensation of the labeled OAA and acetyl-CoA species derived from the ACL-ME pathway, glycolysis, and the TCA cycle produces $^{13}C_3$ to $^{13}C_6$-citrate (light blue circles, Figure S2D). In particular, the presence of the $^{13}C_6$-citrate isotopologue unambiguously confirmed the production of fully labeled acetyl-CoA from the glutamine tracer via the ACL-ME-PDH pathway. Labeled acetyl-CoA production from the ACL reaction is further supported by ^{13}C label incorporation into lipids such as triacylglycerides (TAGs) and phosphatidylcholines (PCs) (Figure S2E).

The $^{13}C_3$- and $^{13}C_5$-citrate isotopologues can also be formed from the ACL-ME plus pyruvate carboxylase (PC) reactions (green circles, Figure S2D). Pyruvate carboxylase is active in P493 cells, as evidenced from the labeled glucose tracer experiment described above (Figure 2). The operation of the ACL-ME1-PDH and ACL-ME1-PC pathways is further corroborated by the production of $^{13}C_3$-succinate, -fumarate, and -malate, which cannot be formed from labeled glutamine via the TCA cycle activity alone. Finally, the production of $^{13}C_5$-citrate from the glutamine tracer can also be explained by reductive carboxylation of αKG to form citrate (orange circles, Figure S2D),

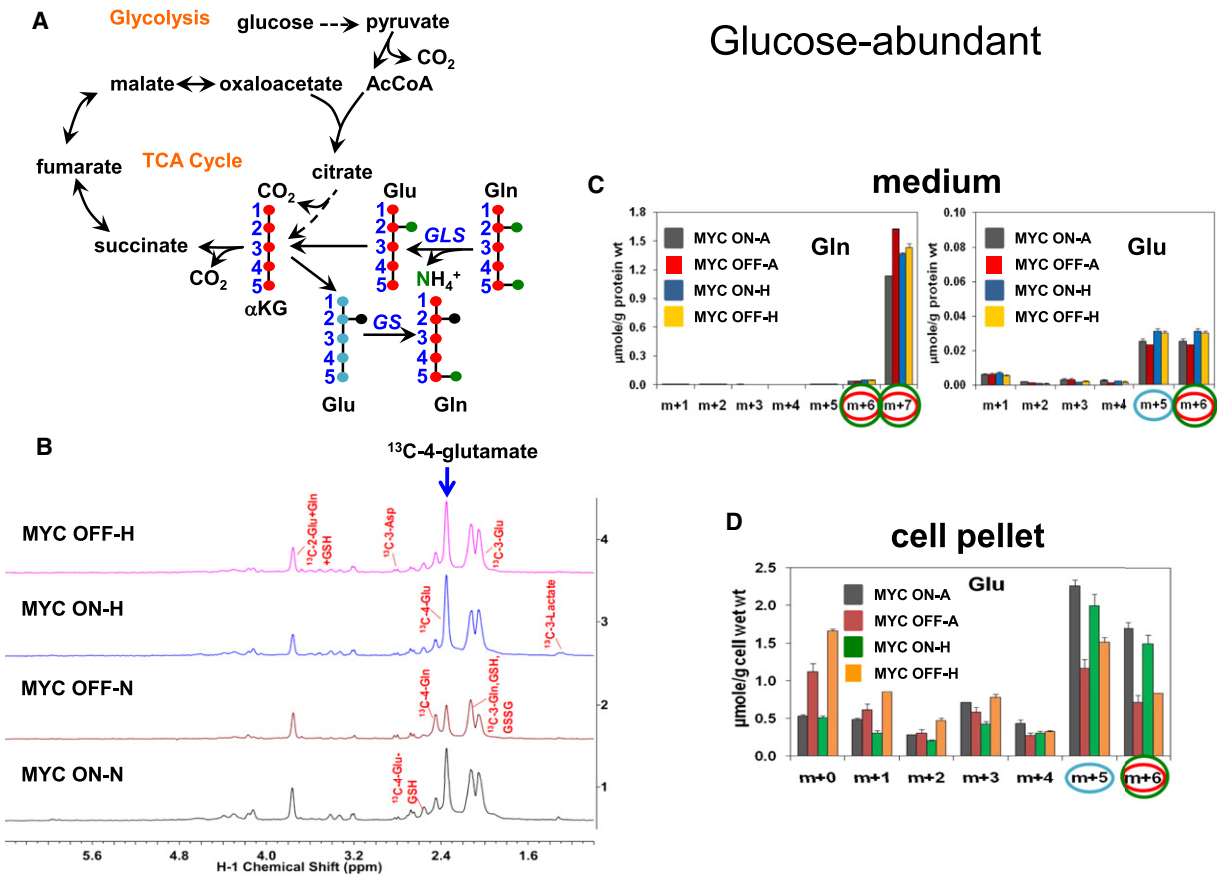

Figure 3. MYC Induces Glutamine to Glutamate Conversion that Persists in Hypoxia

(A) Diagram of ^{13}C labeling patterns products with $^{13}C_5$,$^{15}N_2$-Gln as tracer. Glutamine is labeled at all five carbon and both nitrogen atoms. Glutaminase (GLS) activity produces glutamate $^{13}C^{15}N_1$ with the loss of the amido nitrogen as ammonia. Red and green circles, respective ^{13}C and ^{15}N labeling of glutamate from the glutaminase reaction; light blue circles, ^{13}C labeling of glutamate from the transamination of α-ketoglutarate; black, unlabeled N; GS, glutamine synthetase.

(B) 1-D $^{1}H\{^{13}C\}$ HSQC NMR spectra of cell extracts of P493 MYC ON versus MYC OFF. Intracellular ^{13}C-4-glutamate production from glutamine was reduced when MYC is off in aerobic condition. The conversion of glutamine to glutamate in hypoxia was as high as aerobic condition regardless of MYC expression. NMR spectra were recorded at 800 MHz and 20°C. Each ^{1}H peak arose from protons directly attached to ^{13}C, and the peak assignment denotes the ^{13}C-carbon. The peak intensity reflects ^{13}C abundance of the attached carbon.

(C) Glutamine levels in the media. P493 cells were treated with 0.1 μg/ml tetracycline (MYC OFF) or without tetracycline (MYC ON) for 48 hr in hypoxic (H) or aerobic (A) conditions and were grown in $^{13}C_5$,$^{15}N_2$-Gln (m+7) medium in the presence or absence of tetracycline for 24 hr. Media metabolites were analyzed by GC-MS. Under aerobic conditions, glutamine consumption was decreased when MYC is off. Under hypoxia, glutamine consumption was decreased. The metabolite concentration was expressed as μmole/g protein dry weight.

(D) GC-MS analysis of intracellular conversion of $^{13}C_5$,$^{15}N_2$-glutamine to glutamate. The m+5 glutamate was primarily $^{13}C_5$-glutamate (cf. Figure S1E) with no ^{15}N label, which is derived from $^{13}C_5$-αKG via transamination. The data shown in (B)–(D) were performed three times. The error bars represent SEM.

a reversal of the citrate to αKG reaction catalyzed by aconitase and IDH as recently reported in other cells (Metallo et al., 2011; Mullen et al., 2011; Wise et al., 2011; Yoo et al., 2008) and driven by the hydrolysis of ATP via citrate lyase and ACC. There is abundant CO_2/HCO_3^- in cell culture for reductive carboxylation and presumably in tissue from a number of decarboxylation reactions. However, the relative proportion of the m+5 versus m+3, m+4, and m+6 species, which are characteristic of the forward reactions in the Krebs cycle plus pyruvate carboxylase activity, indicates that reductive carboxylation is not the major pathway in P493 cells, especially under aerobic conditions in which the ratio of αKG to citrate concentration was very low (Figure 4); a high ratio is important for driving this thermodynamically uphill reaction.

We were also intrigued by the apparent upregulation of such TCA cycle-mediated glutamine metabolism by MYC and its persistence under hypoxia (Figure 4). Such a glucose-independent TCA cycle activity would be advantageous for cancer cells subjected to glucose deficiency and/or hypoxia in the tumor microenvironment. Thus, we next determined whether the glutamine-mediated TCA cycle can operate in the absence of glucose and whether glutamine metabolism alone can sustain cell growth and survival.

P493 cells were grown in the absence of glucose using the tracer [U-^{13}C,^{15}N]-Gln to determine whether TCA cycle intermediates could be derived solely from glutamine (Figure 5). In the absence of glucose, the P493 cells completed one doubling in 3 days under aerobic conditions with MYC ON compared with

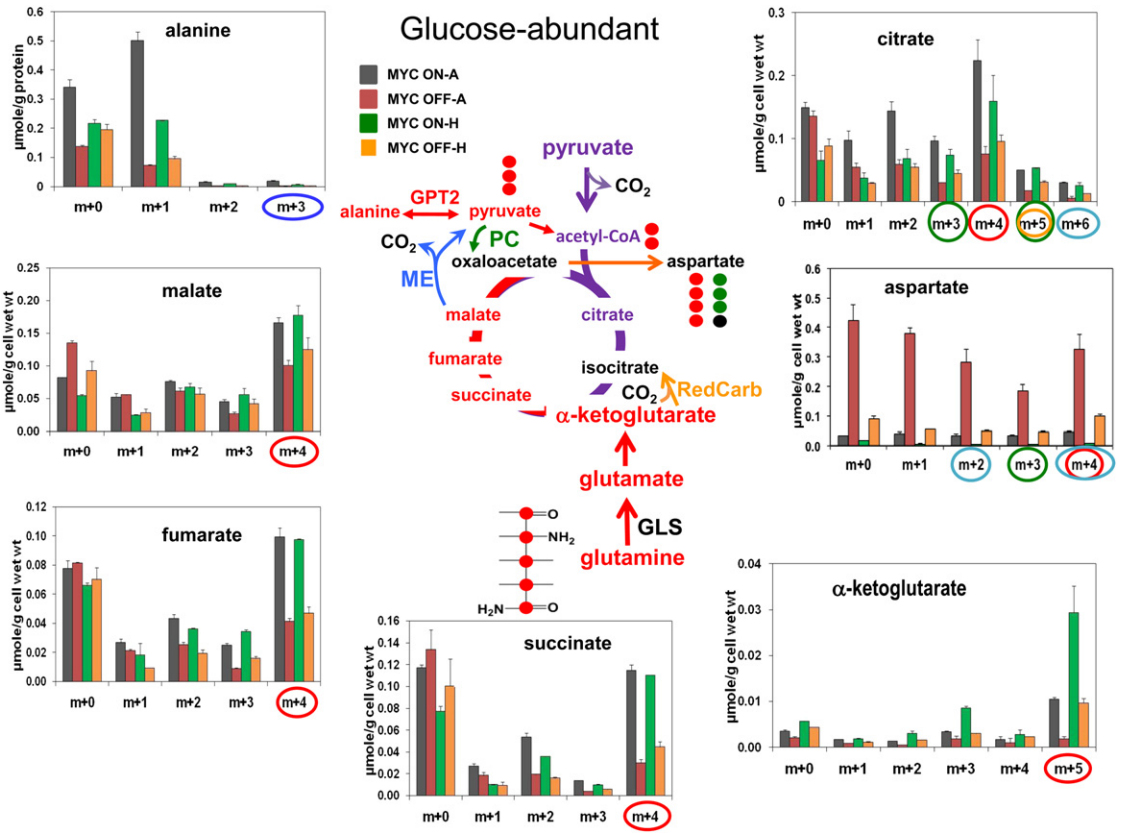

Figure 4. P493 Cells Were Grown in $^{13}C_5$,$^{15}N_2$-Glutamine Medium with Glucose

MYC induces glutamine entry into the TCA cycle, which persists in hypoxia. $^{13}C_5$,$^{15}N_2$ glutamine enters the Krebs cycle to produce α-ketoglutarate, succinate, fumarate, and malate. Citrate can be generated by reductive carboxylation (RedCarb) of glutamine-derived α-ketoglutarate (m+5) (orange circles) or via the forward reactions of the cycle. Malic enzyme (ME) catalyzes the oxidative decarboxylation of malate to pyruvate (light blue). This pyruvate pool (m+3) can be a precursor for both m+2 acetyl-CoA and m+3 OAA (from pyruvate carboxylation, green circles) to make m+5 citrate. The citrate m+6 isotopologue could only arise from glutamine-derived m+4 oxaloacetate (from forward cycle reactions, red circles) and m+2 acetyl-CoA (mediated by malic enzyme). The isotopologue distributions were determined by GC-MS. Each value is an average of duplicate samples. The data shown were performed three times. GPT2, glutamate-pyruvate transaminase; ME, malic enzyme; PC, pyruvate carboxylase; GLS, glutaminase; CO_2 indicates where carbon dioxide is released. A, aerobic; H, hypoxic. The error bars represent SEM.

doubling every 34 ± 2 hr in the presence of glucose (Figure S3A). The cells consumed glutamine (Figure S3B) to produce $^{13}C_5$-αKG (m+5) in a MYC-dependent fashion (circled red, Figure 5). The continued functioning of the TCA cycle under glucose-deprived conditions was identified by the production of various isotopologues of fumarate, malate, and aspartate, particularly the $^{13}C_4$-isotopologues (m+4, Figure 5). However, these labeled isotopologues accumulated to much higher levels (>100-fold for $^{13}C_4$-Asp) than under glucose-replete conditions (compare Figures 4 and 5 or Figure 1B and Figure S3C). This could result from a lower supply of acetyl-CoA under glucose-deprived conditions such that excess glutamine-derived OAA was transaminated to form aspartate. This is also consistent with the lower levels of labeled citrate and αKG isotopologues in glucose-deprived cells than those found in glucose-replete cells (Figures 4 and 5). In the absence of glucose, it is also notable that ^{13}C incorporation from the glutamine tracer into all TCA cycle intermediates decreased under hypoxia but increased with MYC OFF (Figure 5). Furthermore, the ^{13}C alanine isotopologues (e.g., $^{13}C_3$-Ala or m+3 in Figure 5) showed the opposite behavior in response to MYC expression, regardless of the O_2 conditions. The significant buildup of labeled alanine was in contrast to a small production of lactate from glutamine (Figure S3C), which again argues against the operation of the canonical glutamine to lactate pathway in P493 cells.

The relatively low accumulation of labeled TCA metabolites with MYC ON under glucose deprivation could be caused by a combination of limited TCA cycling and the demands for cell proliferation and cell maintenance. The same argument could also apply to aerobic versus hypoxic conditions. In Figure S3A, the highest proliferation rate was observed under aerobic conditions with MYC ON, followed by MYC OFF under aerobic conditions, whereas under hypoxia there was little proliferation regardless of the MYC status. With a slowdown of TCA cycling due to glucose deficiency, a higher consumption rate of labeled TCA intermediates for cell proliferation could deplete these metabolites for both MYC ON and MYC OFF, but more so for MYC ON than MYC OFF and with more depletion under aerobic than hypoxic conditions (Figure 5). Diversion of glutamine for maintenance purposes, e.g., glutathione synthesis for

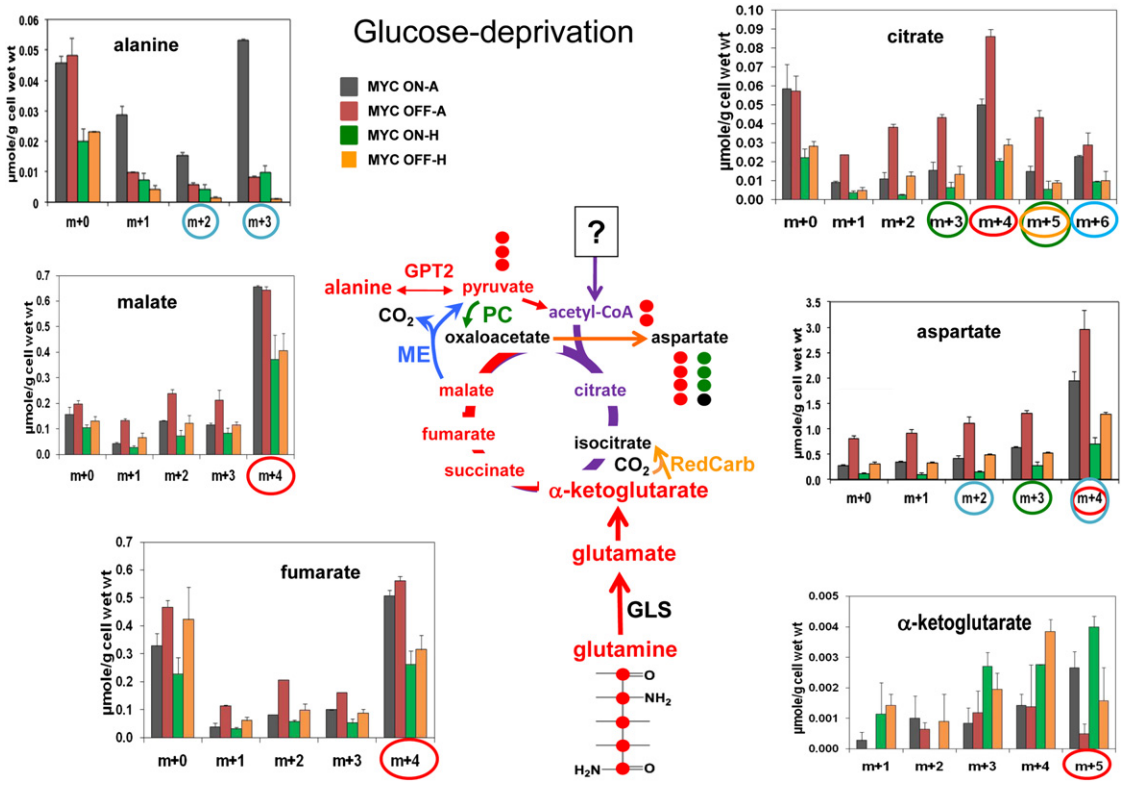

Figure 5. Glutamine-Driven Glucose-Independent TCA Cycle

P493 cells were grown in $^{13}C_5$,$^{15}N_2$-glutamine medium without glucose. The isotopologue distributions were determined by GC-MS. Under glucose-deprived conditions, the m+5 α-ketoglutarate from labeled glutamine was produced in a MYC-dependent fashion. Labeled glutamine was also incorporated into m+4 isotopologues of fumarate and malate downstream of α-ketoglutarate. These isotopologues decreased under hypoxia but not with decreased MYC. The m+3 alanine isotopologue, which is derived from the transamination of glutamine-derived m+3 pyruvate (via malic enzyme), was highly elevated under high MYC and aerobic conditions. Each value is an average of duplicate samples. Colored circles denote the same sets of reactions as in Figure 4. GPT2, glutamate-pyruvate transaminase; ME, malic enzyme; PC, pyruvate carboxylase; GLS, glutaminase; CO_2 indicates where carbon dioxide is released. A, aerobic; H, hypoxic. The error bars represent SEM.

ROS detoxification (inferred by increased ROS production with BPTES inhibition of glutaminolysis, Figure S4A) could also lead to less flux through the TCA cycle. This is consistent with a higher buildup of glutamine-derived glutathione with aerobic and MYC ON conditions (Figure S3C).

When TCA cycling is faster, as in glucose-replete cells, the production rate for the labeled TCA intermediates may be higher than their consumption rate, leading to a higher buildup of these labeled metabolites when MYC is overexpressed (Figure 4). The bottleneck in TCA cycling could also contribute to the significant buildup of $^{13}C_3$-Ala (m+3) alanine under MYC ON and glucose deprivation (Figure 5) via excess production of glutamine-derived pyruvate (by way of the ACL-ME1 pathway, Figure S4), which is transaminated to form alanine via glutamic pyruvic transaminase 1 or 2. Again, this did not occur under glucose-replete conditions, in which glucose, not glutamine, was the main source of alanine production (Figure 2). In the absence of glucose and under hypoxia, P493 cells did not proliferate but continued to consume glutamine and remained viable (Figure S3A).

Under aerobic conditions with MYC ON, the percentages of viable (78% versus 76%) and proliferating (R2, 30.6% versus 30.3%) cell populations were similar between glucose-replete (Figure S6) and -deplete conditions (Figure S7). This can be mediated by the ability of glutamine metabolism to alleviate oxidative stress (Figure S4A) and to support cell bioenergetics (Figure S4B). These data show that when driven by MYC, glutamine plays a crucial role for both cell survival and proliferation under glucose deprivation.

Thus, the above observations confirm a reprogrammed glutamine-dependent TCA cycle that functions in the absence of glucose. Figure S4C outlines the pathways by which ^{13}C carbons of glutamine are converted to labeled acetyl-CoA and reenter the TCA cycle. The significant presence of $^{13}C_5$- (m+5) and $^{13}C_6$-citrate (m+6, Figure 5) is consistent with an ACL-ME-mediated production of acetyl-CoA and citrate solely from glutamine. The ^{13}C labeling of lipid acyl chains, although at relatively low levels (Figure S4D), and the increased labeling under aerobic with MYC ON confirm the activity of ACL and are consistent with the higher rate of proliferation under these conditions (Figure S3A). However, since there was a significant level of unlabeled and $^{13}C_4$-citrate (m+4, Figure 5) under glucose deprivation, there must also be a source(s) of unlabeled acetyl-CoA that contributes to the continued operation of the TCA cycle.

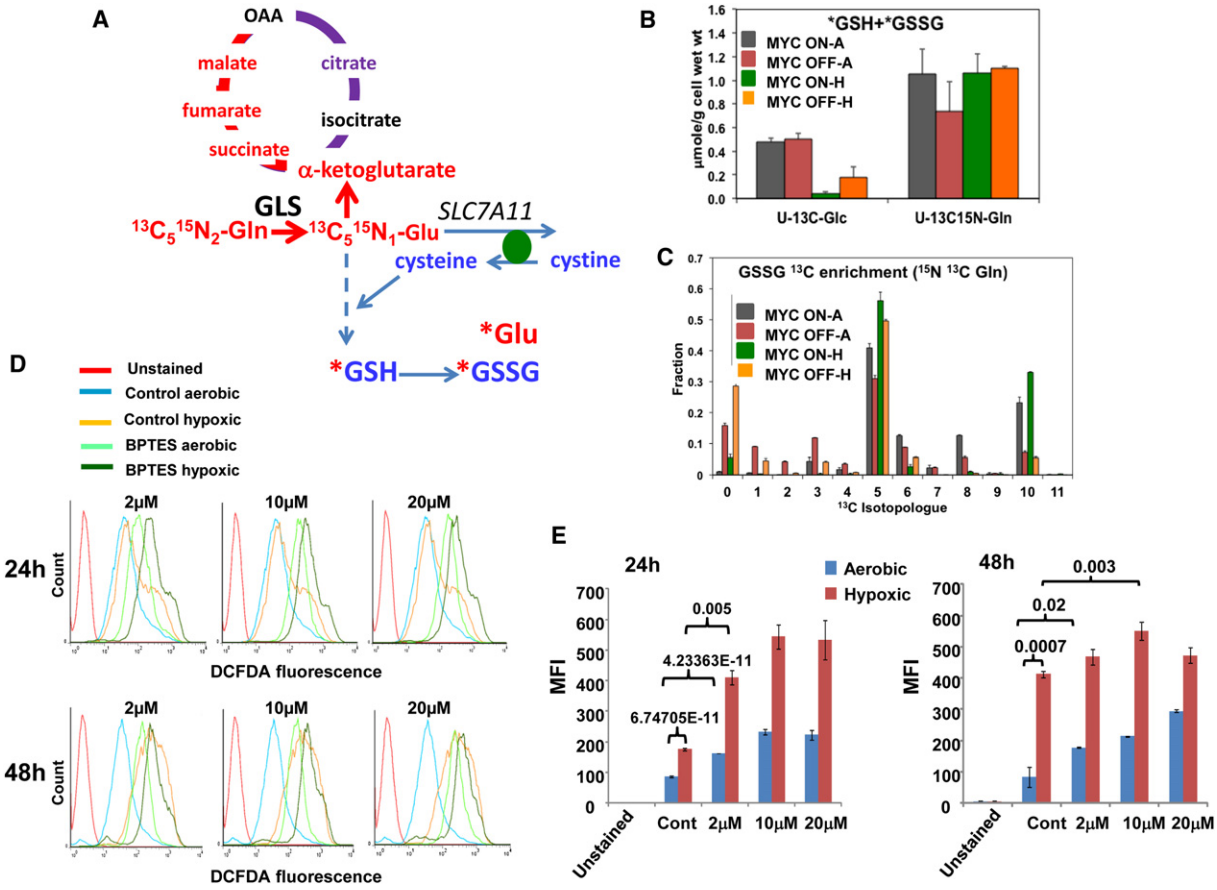

Figure 6. Glutamine Contributes to Glutathione Synthesis and Redox Homeostasis

(A) Diagram of glutamine metabolism to glutathione. Glutamine, when converted to glutamate, is involved in the import of cystine through the antiporter SLC7A11. Cystine is converted to cysteine for the synthesis of glutathione, which also requires glycine and glutamine-derived glutamate.

(B) 1-D $^{1}H\{^{13}C\}$ HSQC NMR analysis of ^{13}C-reduced (*GSH) plus oxidized (*GSSG) glutathiones indicates that the fraction of glutamine contributing to glutathione production was sustained under hypoxia (H) as compared to aerobic condition (A). ^{13}C incorporation was estimated from the ^{13}C-4 peak of the glutamate residue in $GSH^{+}GSSG$ by 1D HSQC NMR.

(C) FT-ICR-MS determination of glutathione oxidation. The $^{13}C_5$ and $^{13}C_{10}$ isotopologues of GSSG were most likely derived from the $^{13}C_5,^{15}N_2$-glutamine tracer via respective incorporation of one and two units of $^{13}C_5$-Glu. The error bars in (B) and (C) represent SEM.

(D) Glutamine-dependent redox homeostasis. Flow cytometric histograms of ROS levels were determined by DCFDA fluorescence in P493 cells treated with 2, 10, and 20 μM BPTES for 24 and 48 hr.

(E) Mean fluorescence intensity (MFI). MFI for DCFDA fluorescence is shown for the different concentrations of BPTES under aerobic and hypoxic conditions. MFI was determined from triplicate experiments with SD and p values (t test) shown.

We have observed that fatty acid oxidation, a possible source for unlabeled acetyl-CoA, increased in the absence of ectopic MYC in P493 cells (Figure S5B). This could account for the higher levels of $^{13}C_4$-citrate when MYC was off (Figure 5). However, it cannot explain the comparable levels of unlabeled citrate (m+0 Figure 5) between aerobic MYC ON and MYC OFF. Therefore other sources of unlabeled acetyl CoA, such as oxidation of amino acids, may also exist.

Glutamine-Dependent Bioenergetics and Redox Homeostasis, a Cell Survival Pathway in Hypoxia

The dependence of P493 cells on glutamine for proliferation and maintenance under aerobic and hypoxic conditions suggests a key role for glutamine in driving anaplerotic and bioenergetic needs of both dividing and resting cells. We found that the interruption of glutamine metabolism with the glutaminase inhibitor BPTES decreased ATP levels under aerobic conditions. In hypoxia, cells maintained a lower ATP level that was further diminished by BPTES treatment (Figure 7B). These results suggest that glutamine metabolism via the glucose-independent TCA cycle supports cellular bioenergetics for cell survival (and proliferation) under both aerobic and hypoxic conditions.

In addition, both dividing and resting cells require redox homeostasis, not only for continuing glycolysis but also for detoxifying ROS. Glutamine, when converted to glutamate, could also be involved in the import of cystine through the antiporter SLC7A11 (Figure 6A). This is consistent with the significant excretion of labeled glutamate into the culture medium (Figure 3C). Cystine, when converted to cysteine, contributes to the synthesis of glutathione together with glycine and glutamate derived from glutamine. We thus determined the contributions of labeled glutamine and glucose to total de novo

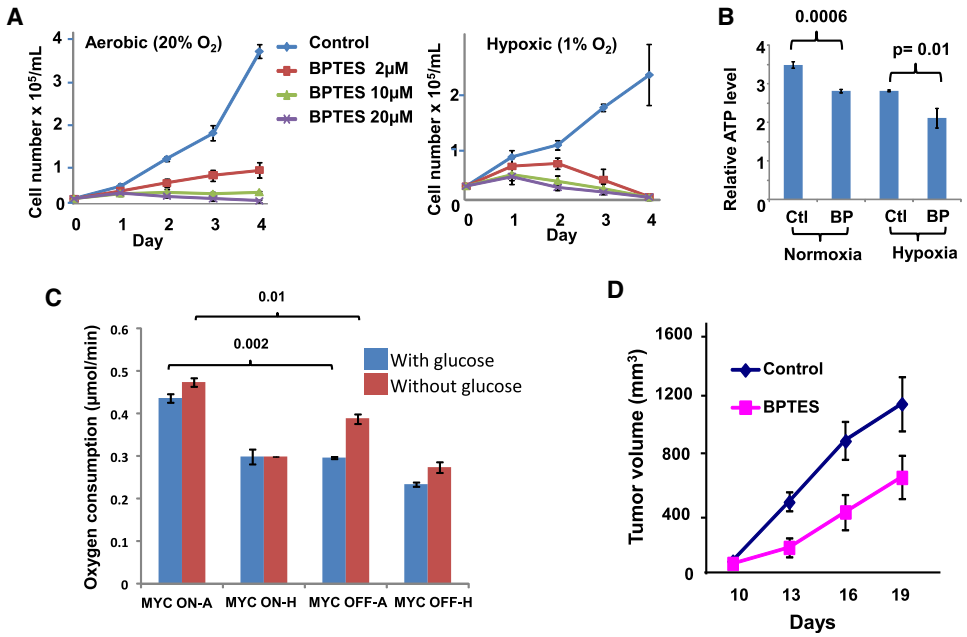

Figure 7. Effects of a Glutaminase Inhibitor on Neoplastic Cells In Vitro and in a Tumor Xenograft Model In Vivo

(A) Effect of glutaminase inhibitor, BPTES, on aerobic and hypoxic P493 cell growth. Growth of control cells compared with cells treated with BPTES under both aerobic and hypoxic conditions. All cells were grown at 1 × 10^5 cells/mL. Cell counts were performed in triplicate and shown as mean ±SD. Live cells were counted daily in a hemocytometer using trypan blue dye exclusion.

(B) Effect of BPTES on steady-state ATP levels. P493 cells were treated with 2 μM BPTES for 20 hr and counted. ATP levels (mean ±SD, n = 3 experiments) were determined by luciferin-luciferase-based assay on aliquots containing an equal number of live cells. *p = 0.0006; **p = 0.01 (t test).

(C) Effects of hypoxia and glucose deprivation on oxygen consumption rates. Oxygen consumption rates of aerobic (A) or hypoxic (H) P493 cells were determined by a Clark-type oxygen electrode after culture in the presence or absence of glucose for 24 hr. Data are from duplicate experiments with SD and p values (t test) shown.

(D) In vivo efficacy of BPTES. 2.0 × 10^7 P493 human lymphoma B cells were injected subcutaneously into tumor-bearing SCID mice. When the tumor volume reached 100 mm^3, 200 μg BPTES was injected every other day by intraperitoneal (i.p.) administration (12.5 mg/kg bodyweight) for 20 days. Control animals were treated with daily i.p. injection of vehicle (2% [vol/vol] DMSO). BPTES inhibited lymphoma xenograft growth as compared to control. The tumor volumes were measured using digital calipers every 4 days and calculated using the following formula: (length [mm] × width [mm] × width [mm] × 0.52). The results represent the average ±SEM (n = 7 each).

glutathione synthesis by quantifying ^{13}C-labeled reduced plus oxidized glutathione levels derived from respective glucose or glutamine tracers (Figure 6B; *GSH-*GSSG). Relative to glucose, glutamine carbons were more readily incorporated into the glutamate moiety of the glutathione, indicating that glutamine, not glucose, is the main precursor for glutathione synthesis. While the glucose carbon contribution to glutathione diminished in hypoxia, the contribution from glutamine carbons persisted. Furthermore, the ^{13}C fractional distribution in oxidized glutathione (GSSG) isotopologues (e.g., m+5 and m+10 in Figure 6C) was in fact higher under hypoxia with MYC ON than under aerobic with MYC OFF, which could reflect a higher ROS production or oxidation of de novo-synthesized glutathione in response to MYC expression and hypoxia. This observation is supported by a lower level of reduced glutathione (GSH) (Figure S5D) and higher ROS production (Figure 6D) in P493 cells under hypoxia and inhibition of glutaminase by BPTES. The order of GSH levels was aerobic control > hypoxic control > aerobic BPTES > > hypoxic BPTES, while that of ROS production (measured by DCFDA fluorescence) was reversed, which is expected for removal of ROS by oxidation of GSH to GSSG.

To determine further the role of glutaminase in redox homeostasis, we isolated T cells from mice that are heterozygous for mitochondrial glutaminase 1 ($Gls^{+/-}$) (Masson et al., 2006), which is the homolog of human kidney type glutaminase rather than liver-specific glutaminase 2. When compared to aerobic and hypoxic wild-type (WT) T cells, the $Gls^{+/-}$ T cells had higher basal ROS levels, which were further increased under hypoxia (Figure S5E). Altogether, these data suggest that MYC expression can enhance aerobic glutathione biosynthesis from glutamine to maintain redox homeostasis. Glutamine-derived glutathione production was also sustained under hypoxia to cope with heightened ROS production from the perturbed mitochondrial electron transport chain (Chandel et al., 1998; Guzy et al., 2005).

Our findings that MYC-induced glutamine metabolism persisted in hypoxia and in the absence of glucose for cell maintenance led us to test whether targeting glutaminase is feasible for cancer therapy. We determined the consequences of BPTES treatment on aerobic and hypoxic P493 cell proliferation (Figure 7A). While BPTES decreased glutaminase activity (Figure S5C) and the proliferation of aerobic P493 cells, inhibition of glutaminase killed hypoxic P493 cells (Figure 7A). Under hypoxia, the cells proliferated less but continued to import and metabolize glutamine (Figure S2C and Figure 4) as well as survive (Figure S6), even under glucose-deprived conditions (Figure S7). The killing effect of BPTES under hypoxia can be

ascribed to the crucial role of glutamine metabolism for survival by supporting cell bioenergetics (Figure 7B) and alleviating oxidative stress (Figure 6). This notion is consistent with the persistent, although diminished, rate of oxygen consumption by hypoxic cells as compared with aerobic cells (Figure 7C). Glucose deprivation increases the rate of oxygen consumption (Figure 7C) as previously reported (Gao et al., 2009). To determine the in vivo significance of our findings, P493 tumor xenograft-bearing mice were treated with intraperitoneal injections of BPTES (Figure 7D). As compared with DMSO vehicle-treated mice, the BPTES-treated mice demonstrated a significantly diminished tumor progression.

DISCUSSION

Although increased glucose metabolism has been hypothesized to drive the bioenergetic needs of cancer cells, it is clear that highly proliferative cancer cells require additional supplies of biosynthetic precursors not met by glucose metabolism; thus there is the requirement of anaplerosis via glutaminolysis and/or pyruvate carboxylation as well as other sources such as fatty acids (DeBerardinis et al., 2007; Deberardinis et al., 2008; Fan et al., 2009; Gao et al., 2009; Wise et al., 2008). A significant proportion of the biosynthetic needs under aerobic conditions may be met by glutamine metabolism, which is regulated by the activity of the *MYC* oncogene (Gao et al., 2009; Wise et al., 2008). In this regard, our previous studies documented the ability of MYC to induce mitochondrial biogenesis, function, and enhanced oxygen consumption (Li et al., 2005), which persisted under hypoxia (Figure 7C). Our data show that the import rates of both glucose and glutamine greatly exceed those of other amino acids under these various experimental conditions, suggesting that they are the major sources for energy and anaplerosis. However, it is a long-standing question how cancer cells survive or even proliferate under the hypoxic and nutrient-deprived conditions encountered in the tumor microenvironment (Schroeder et al., 2005).

Solid tumors are often poorly vascularized, leading to regions of hypoxia and glucose deficiency (Goel et al., 2011; Schroeder et al., 2005), which must be overcome for cancer cells to continue proliferation and survive. Although MYC-overexpressing cells appear to become addicted to glutamine, the heightened addiction to glutamine under hypoxia had not been previously established (Yuneva et al., 2007). We therefore determined how limited oxygen availability would influence glutamine metabolism in vitro to gain insights into what might happen in vivo. It should be noted, however, that our well-controlled cell line studied in vitro may have adapted epigenetically and metabolically to prolonged cultures in nutrient-rich conditions, and hence metabolic changes under our in vitro experimental conditions may be instructive, but may not fully represent what happens in vivo in the tumor microenvironment. Notwithstanding this caveat, we used uniformly labeled [U-^{13}C,^{15}N]-Gln and traced the fate of glutamine carbon and nitrogen atoms in both aerobic and hypoxic conditions with MYC turned OFF or ON in a human B cell model of Burkitt lymphoma (P493). The P493 system is strictly dependent on MYC function for cell proliferation; as such, this experimental model does not conclusively allow us to distinguish the metabolic consequences of MYC-mediated transcriptional changes versus those that occur due to changes in cell size increase or proliferative status as previously reported (Schuhmacher et al., 1999). We surmise that most of the metabolic changes between MYC ON and MYC OFF states are consequential to MYC regulation of genes involved in both glucose and glutamine metabolism as previously documented (Dang et al., 2009a). The entry of glutamine, after its conversion to glutamate and then to α-ketoglutarate, into the TCA and oxidation to succinate, fumarate, and malate were highly facilitated by MYC expression. More intriguingly, glutamine metabolism via the TCA cycle persisted under hypoxia and remained responsive to MYC. Based on detailed analyses of ^{13}C isotopologues of citrate, succinate, fumarate, and malate (Figure 4), we uncovered a glucose-independent TCA cycle solely supported by glutamine, which involved the supply of acetyl-CoA and OAA to the TCA cycle by the combined activity of ATP citrate lyase, ME, PDH, and/or pyruvate carboxylase (Figure 4). This pathway was operative even when glucose was abundant and remained active under hypoxia. These data collectively define a more efficient pathway of glutaminolysis, in which glutamine can be used either for anabolic purposes for proliferation, or for producing energy. This pathway can produce up to 17.5 mol ATP/mol glutamine oxidized to CO_2. This is in contrast to the canonical glutaminolysis pathway from glutamine to lactate (Helmlinger et al., 2002; Newsholme et al., 1985a, 1985b), in which the glutamine carbons are not oxidized via the TCA cycle and produce only 5 ATP/mol glutamine converted to lactate + CO_2.

To further explore the role of the glucose-independent TCA cycle, we traced glutamine metabolism under glucose-deprived culture conditions. SIRM analysis of TCA cycle metabolites revealed a relative increase in this glutamine-mediated pathway in glucose-deprived conditions, as evidenced by the increase in the ratios of $^{13}C_6$-citrate and $^{13}C_5$-citrate to $^{13}C_4$-citrate (Figure 5). The metabolites produced through this glutamine pathway provided the anabolic precursors (citrate) for lipid synthesis (Figure S4D) and cell survival precursor (Glu) for glutathione production (Figure 6B, Figure S3C), which was commensurate with the aerobic growth demand (Figure S3A) and the need for ROS quenching under hypoxia (Figure 6). These observations are consistent with our previous findings that knockdown of glutaminase by siRNA resulted in increased ROS and slowed growth that could be partially rescued by N-acetylcysteine (Gao et al., 2009). It is also notable that pyruvate carboxylase plays a significant role in this glutamine pathway (Figures 4 and 5) and that glutamine-independent tumor cells use pyruvate carboxylase to drive a glucose-dependent TCA cycle in the absence of glutamine (Cheng et al., 2011). Thus, the flexibility of the TCA cycle to use either or both anaplerotic pathways may be important for tumor adaptation. More practically, therapeutic approaches targeting metabolism must consider these adaptive strategies.

As a proof of concept, we tested the effect of a glutaminase inhibitor (BPTES) on growth and ROS production of P493 cells and showed that blocking glutamine metabolism not only inhibited tumor cell growth under aerobic conditions but also led to cell death under hypoxia and reduction of tumor xenograft growth in vivo (Figures 7A and 7D). The specificity of BPTES was previously documented by our studies in glioma cells, which

revealed BPTES-induced metabolic changes, such as diminished glutamate, α-ketoglutarate, succinate, fumarate, and malate levels, consistent with an on-target effect on glutaminase (Seltzer et al., 2010). Further, the uncompetitive nature of BPTES inhibitory activity was recently underscored by the crystal structure of glutaminase (GAC form) cocrystallized with BPTES, which sits at the oligomerization interface of the glutaminase tetramer (Delabarre et al., 2011). Our finding of a glutamine-driven TCA cycle and other recent discoveries of cancer-related metabolic pathways (Dang et al., 2009b; Frezza et al., 2011; Possemato et al., 2011) suggest that metabolic flexibility may be a common feature of tumor cell metabolism. Hence, a broader and deeper understanding of cancer cell metabolism and their ability to reprogram canonical biochemical pathways under metabolic stress can be a rich ground for uncovering strategies for therapeutic targeting of tumors.

EXPERIMENTAL PROCEDURES

Detailed materials and methods are available online in the Supplemental Information.

^{13}C-Labeled Glutamine or Glucose and Hypoxic Exposure

Briefly, Human lymphoma B P493 cells were grown in [U-^{13}C]-labeled glucose or [U-^{13}C,^{15}N]-labeled glutamine for 24 hr. Nonhypoxic cells (21% [(vol/vol] O_2) were maintained at 37°C in a 5% (vol/vol) CO_2 and 95% (vol/vol) air incubator. Hypoxic cells (1% O_2) were maintained in a controlled atmosphere chamber (PLAS-LABS) with a gas mixture containing 1% O_2, 5% (vol/vol) CO_2, and 94% (vol/vol) N_2 at 37°C for 48 hr. Metabolites were extracted from cells and media as previously described (Fan et al., 2011).

Bromobimane and carboxy-H2DCFDA were used to measure reduced glutathione ROS levels, respectively, using flow cytometry.

ATP Levels

ATP levels were determined by luciferin-luciferase-based assay (Promega).

Glutaminase Activity

Cells treated with BPTES and/or tetracycline were then incubated with [^{3}H] glutamine to assess glutaminase activity.

The β-oxidation of 14C labeled oleic acid was used to assess fatty acid oxidation.

Cell Viability Assay

The presence of dead cells was determined by propidium iodide staining at 2 μg/ml using flow cytometry.

Statistical Analysis

Values are shown as mean ± standard deviation (SD) or standard error of the mean (SEM). Data were analyzed using the Student's t test, and significance was defined as $p < 0.05$.

SUPPLEMENTAL INFORMATION

Supplemental Information includes seven figures, one table, Supplemental Experimental Procedures, and Supplemental References and can be found with this article online at doi:10.1016/j.cmet.2011.12.009.

ACKNOWLEDGMENTS

This work was supported by in part by grant 1R21NS074151-01 (to T.T.); The Sol Goldman Pancreatic Cancer Research fund (to A.L.); grants 5R01CA051497-21 and 5R01CA057341-20, Leukemia Lymphoma Society grant LLS-6363-11, and Stand-Up-to-Cancer/American Association for Cancer Research translational grant (to C.V.D.); grants 1R01CA118434-01A2 and 3R01CA118434-02S1, University of Louisville CTSPGP grants 20044 (to T.W.M.F.) and 20061 (to A.N.L.); and National Institutes of Health National Center for Research Resources (NIH NCRR) grant 5P20RR018733, Kentucky Challenge for Excellence, the Brown Foundation, and Kentucky Lung Cancer Research Program (postdoctoral fellowship to P.K.L.). The FT-ICR-MS instrumentation was supported by the National Science Foundation's Office of Experimental Program to Stimulate Competitive Research (NSF/EPSCoR) grant number EPS-0447479. We thank Ramani Dinavahi, Julie Tan, and Radhika Burra for excellent technical assistance and Stephen Rayport for the heterozygous glutaminase mice. A.L., A.N.L., T.W.M.F., and C.V.D. designed research and wrote the manuscript. A.L., A.N.L., M.H., S.B., J.B., C.J.R., H.Z., L.J.Z., R.J.C.S., P.K.L., R.M.H., and T.W.M.F. performed research; all authors interpreted the data and commented on the manuscript.

Received: November 3, 2011
Revised: December 8, 2011
Accepted: December 14, 2011
Published online: January 3, 2012

REFERENCES

Bensaad, K., Tsuruta, A., Selak, M.A., Vidal, M.N., Nakano, K., Bartrons, R., Gottlieb, E., and Vousden, K.H. (2006). TIGAR, a p53-inducible regulator of glycolysis and apoptosis. Cell *126*, 107–120.

Chandel, N.S., Maltepe, E., Goldwasser, E., Mathieu, C.E., Simon, M.C., and Schumacker, P.T. (1998). Mitochondrial reactive oxygen species trigger hypoxia-induced transcription. Proc. Natl. Acad. Sci. USA *95*, 11715–11720.

Cheng, T., Sudderth, J., Yang, C., Mullen, A.R., Jin, E.S., Mates, J.M., and DeBerardinis, R.J. (2011). Pyruvate carboxylase is required for glutamine-independent growth of tumor cells. Proc. Natl. Acad. Sci. USA *108*, 8674–8679.

Dang, C.V. (2010). Rethinking the Warburg effect with Myc micromanaging glutamine metabolism. Cancer Res. *70*, 859–862.

Dang, C.V., Le, A., and Gao, P. (2009a). MYC-induced cancer cell energy metabolism and therapeutic opportunities. Clin. Cancer Res. *15*, 6479–6483.

Dang, L., White, D.W., Gross, S., Bennett, B.D., Bittinger, M.A., Driggers, E.M., Fantin, V.R., Jang, H.G., Jin, S., Keenan, M.C., et al. (2009b). Cancer-associated IDH1 mutations produce 2-hydroxyglutarate. Nature *462*, 739–744.

Dang, L., Jin, S., and Su, S.M. (2010). IDH mutations in glioma and acute myeloid leukemia. Trends Mol. Med. *16*, 387–397.

DeBerardinis, R.J., Mancuso, A., Daikhin, E., Nissim, I., Yudkoff, M., Wehrli, S., and Thompson, C.B. (2007). Beyond aerobic glycolysis: transformed cells can engage in glutamine metabolism that exceeds the requirement for protein and nucleotide synthesis. Proc. Natl. Acad. Sci. USA *104*, 19345–19350.

Deberardinis, R.J., Sayed, N., Ditsworth, D., and Thompson, C.B. (2008). Brick by brick: metabolism and tumor cell growth. Curr. Opin. Genet. Dev. *18*, 54–61.

Delabarre, B., Gross, S., Fang, C., Gao, Y., Jha, A., Jiang, F., Song, J.J., Wei, W., and Hurov, J.B. (2011). Full-length human glutaminase in complex with an allosteric inhibitor. Biochemistry *50*, 10764–10770.

Fan, T.W., Lane, A.N., Higashi, R.M., Farag, M.A., Gao, H., Bousamra, M., and Miller, D.M. (2009). Altered regulation of metabolic pathways in human lung cancer discerned by 13C stable isotope-resolved metabolomics (SIRM). Mol. Cancer *8*, 41.

Fan, T.W.-M., Yuan, P., Lane, A.N., Higashi, R.M., Wang, Y., Hamidi, A., Zhou, R., Guitart-Navarro, X., Chen, G., Manji, H.K., et al. (2010). Stable isotope resolved metabolomic analysis of lithium effects on glial-neuronal interactions. Metabolomics *6*, 165–179.

Fan, T.W.-M., Lane, A.N., Higashi, R.M., and Yan, J. (2011). Stable isotope resolved metabolomics of lung cancer in a scid mouse model. Metabolomics *7*, 257–269.

Frezza, C., Zheng, L., Folger, O., Rajagopalan, K.N., MacKenzie, E.D., Jerby, L., Micaroni, M., Chaneton, B., Adam, J., Hedley, A., et al. (2011). Haem oxygenase is synthetically lethal with the tumour suppressor fumarate hydratase. Nature. 10.1038/nature10363.

Gao, P., Tchernyshyov, I., Chang, T.C., Lee, Y.S., Kita, K., Ochi, T., Zeller, K.I., De Marzo, A.M., Van Eyk, J.E., Mendell, J.T., et al. (2009). c-Myc suppression

of miR-23a/b enhances mitochondrial glutaminase expression and glutamine metabolism. Nature *458*, 762–765.

Goel, S., Duda, D.G., Xu, L., Munn, L.L., Boucher, Y., Fukumura, D., and Jain, R.K. (2011). Normalization of the vasculature for treatment of cancer and other diseases. Physiol. Rev. *91*, 1071–1121.

Guzy, R.D., Hoyos, B., Robin, E., Chen, H., Liu, L., Mansfield, K.D., Simon, M.C., Hammerling, U., and Schumacker, P.T. (2005). Mitochondrial complex III is required for hypoxia-induced ROS production and cellular oxygen sensing. Cell Metab. *1*, 401–408.

Helmlinger, G., Sckell, A., Dellian, M., Forbes, N.S., and Jain, R.K. (2002). Acid production in glycolysis-impaired tumors provides new insights into tumor metabolism. Clin. Cancer Res. *8*, 1284–1291.

Kim, J.W., Tchernyshyov, I., Semenza, G.L., and Dang, C.V. (2006). HIF-1-mediated expression of pyruvate dehydrogenase kinase: a metabolic switch required for cellular adaptation to hypoxia. Cell Metab. *3*, 177–185.

Kim, J.W., Gao, P., Liu, Y.C., Semenza, G.L., and Dang, C.V. (2007). Hypoxia-inducible factor 1 and dysregulated c-Myc cooperatively induce vascular endothelial growth factor and metabolic switches hexokinase 2 and pyruvate dehydrogenase kinase 1. Mol. Cell. Biol. *27*, 7381–7393.

Kim, J., Lee, J.H., and Iyer, V.R. (2008). Global identification of Myc target genes reveals its direct role in mitochondrial biogenesis and its E-box usage in vivo. PLoS One *3*, e1798. 10.1371/journal.pone.0001798.

King, A., Selak, M.A., and Gottlieb, E. (2006). Succinate dehydrogenase and fumarate hydratase: linking mitochondrial dysfunction and cancer. Oncogene *25*, 4675–4682.

Koppenol, W.H., Bounds, P.L., and Dang, C.V. (2011). Otto Warburg's contributions to current concepts of cancer metabolism. Nat. Rev. Cancer *11*, 325–337.

Li, F., Wang, Y., Zeller, K.I., Potter, J.J., Wonsey, D.R., O'Donnell, K.A., Kim, J.W., Yustein, J.T., Lee, L.A., and Dang, C.V. (2005). Myc stimulates nuclearly encoded mitochondrial genes and mitochondrial biogenesis. Mol. Cell. Biol. *25*, 6225–6234.

Masson, J., Darmon, M., Conjard, A., Chuhma, N., Ropert, N., Thoby-Brisson, M., Foutz, A.S., Parrot, S., Miller, G.M., Jorisch, R., et al. (2006). Mice lacking brain/kidney phosphate-activated glutaminase have impaired glutamatergic synaptic transmission, altered breathing, disorganized goal-directed behavior and die shortly after birth. J. Neurosci. *26*, 4660–4671.

Metallo, C.M., Gameiro, P.A., Bell, E.L., Mattaini, K.R., Yang, J., Hiller, K., Jewell, C.M., Johnson, Z.R., Irvine, D.J., Guarente, L., et al. (2011). Reductive glutamine metabolism by IDH1 mediates lipogenesis under hypoxia. Nature. Published online November 20, 2011. 10.1038/nature10602.

Mullen, A.R., Wheaton, W.W., Jin, E.S., Chen, P.H., Sullivan, L.B., Cheng, T., Yang, Y., Linehan, W.M., Chandel, N.S., and Deberardinis, R.J. (2011). Reductive carboxylation supports growth in tumour cells with defective mitochondria. Nature. Published online November 20, 2011. 10.1038/nature10642.

Newsholme, E.A., Crabtree, B., and Ardawi, M.S. (1985a). Glutamine metabolism in lymphocytes: its biochemical, physiological and clinical importance. Q. J. Exp. Physiol. *70*, 473–489.

Newsholme, E.A., Crabtree, B., and Ardawi, M.S. (1985b). The role of high rates of glycolysis and glutamine utilization in rapidly dividing cells. Biosci. Rep. *5*, 393–400.

Possemato, R., Marks, K.M., Shaul, Y.D., Pacold, M.E., Kim, D., Birsoy, K., Sethumadhavan, S., Woo, H.-K., Jang, H.G., Jha, A.K., et al. (2011). Functional genomics reveal that the serine synthesis pathway is essential in breast cancer. Nature *476*, 345–350.

Robinson, M.M., McBryant, S.J., Tsukamoto, T., Rojas, C., Ferraris, D.V., Hamilton, S.K., Hansen, J.C., and Curthoys, N.P. (2007). Novel mechanism of inhibition of rat kidney-type glutaminase by bis-2-(5-phenylacetamido-1,2,4-thiadiazol-2-yl)ethyl sulfide (BPTES). Biochem. J. *406*, 407–414.

Samudio, I., Fiegl, M., and Andreeff, M. (2009). Mitochondrial uncoupling and the Warburg effect: molecular basis for the reprogramming of cancer cell metabolism. Cancer Res. *69*, 2163–2166.

Schroeder, T., Yuan, H., Viglianti, B.L., Peltz, C., Asopa, S., Vujaskovic, Z., and Dewhirst, M.W. (2005). Spatial heterogeneity and oxygen dependence of glucose consumption in R3230Ac and fibrosarcomas of the Fischer 344 rat. Cancer Res. *65*, 5163–5171.

Schuhmacher, M., Staege, M.S., Pajic, A., Polack, A., Weidle, U.H., Bornkamm, G.W., Eick, D., and Kohlhuber, F. (1999). Control of cell growth by c-Myc in the absence of cell division. Curr. Biol. *9*, 1255–1258.

Seltzer, M.J., Bennett, B.D., Joshi, A.D., Gao, P., Thomas, A.G., Ferraris, D.V., Tsukamoto, T., Rojas, C.J., Slusher, B.S., Rabinowitz, J.D., et al. (2010). Inhibition of glutaminase preferentially slows growth of glioma cells with mutant IDH1. Cancer Res. *70*, 8981–8987.

Telang, S., Lane, A.N., Nelson, K.K., Arumugam, S., and Chesney, J.A. (2007). The oncoprotein H-RasV12 increases mitochondrial metabolism. Mol. Cancer *6*, 77.

Vander Heiden, M.G. (2011). Targeting cancer metabolism: a therapeutic window opens. Nat. Rev. Drug Discov. *10*, 671–684.

Vander Heiden, M.G., Cantley, L.C., and Thompson, C.B. (2009). Understanding the Warburg effect: the metabolic requirements of cell proliferation. Science *324*, 1029–1033.

Warburg, O. (1956). On the origin of cancer cells. Science *123*, 309–314.

Warburg, O., Posener, K., and Negelein, E. (1924). Ueber den Stoffwechsel der Tumoren. Biochem. Z. *152*, 319–344.

Wise, D.R., DeBerardinis, R.J., Mancuso, A., Sayed, N., Zhang, X.Y., Pfeiffer, H.K., Nissim, I., Daikhin, E., Yudkoff, M., McMahon, S.B., et al. (2008). Myc regulates a transcriptional program that stimulates mitochondrial glutaminolysis and leads to glutamine addiction. Proc. Natl. Acad. Sci. USA *105*, 18782–18787.

Wise, D.R., Ward, P.S., Shay, J.E., Cross, J.R., Gruber, J.J., Sachdeva, U.M., Platt, J.M., Dematteo, R.G., Simon, M.C., and Thompson, C.B. (2011). Hypoxia promotes isocitrate dehydrogenase-dependent carboxylation of alpha-ketoglutarate to citrate to support cell growth and viability. Proc. Natl. Acad. Sci. USA *108*, 19611–19616.

Wu, W., Platoshyn, O., Firth, A.L., and Yuan, J.X. (2007). Hypoxia divergently regulates production of reactive oxygen species in human pulmonary and coronary artery smooth muscle cells. Am. J. Physiol. Lung Cell. Mol. Physiol. *293*, L952–L959.

Yoo, H., Antoniewicz, M.R., Stephanopoulos, G., and Kelleher, J.K. (2008). Quantifying reductive carboxylation flux of glutamine to lipid in a brown adipocyte cell line. J. Biol. Chem. *283*, 20621–20627.

Yuneva, M., Zamboni, N., Oefner, P., Sachidanandam, R., and Lazebnik, Y. (2007). Deficiency in glutamine but not glucose induces MYC-dependent apoptosis in human cells. J. Cell Biol. *178*, 93–105.